Star formation histories of LSB dwarf irregular galaxies in the Virgo cluster

Ana B. Heller, Elchanan Almoznino and Noah Brosch

The Wise Observatory and the School of Physics and Astronomy

Tel Aviv University, Tel Aviv 69978, Israel

1. Abstract

The star formation (SF) histories of low surface brightness, dwarf irregular galaxies (LSB-dIs) in the Virgo cluster (VC) are investigated using Hα and broad-band optical colors. Models derived from published libraries of evolutionary synthesis models are employed to describe the observed colors. The results show that the simplest models cannot explain the evolution of these galaxies. The relative flux contribution of the young and the old population is constrained by a novel flux-weighted scheme and indicative metallicities are derived from the best fit photometric models. We find that LSB-dIs cannot be the faded remains of star-bursting dwarf galaxies and also cannot be objects where a low-key continuous star formation process takes place. A more likely explanation is that in LSB-dIs episodic star formation takes place, at a lower intensity than in Blue Compact dwarf galaxies (BCDs).

2. Introduction

Dwarf galaxies have $M_B \geq -18$ and can be classified morphologically as dE, dSp, or dI. The last class, dwarf irregulars, was studied in detail in our series of papers (Heller *et al.*, 1998, 1999, 2000, 2001) where the emphasis was on surface photometry of low surface brightness dwarf (LSB-dIs) irregulars of Virgo Cluster members with B-band central surface brightness $\mu_0 > 23.0$ mag arcsec^{-2}. Our results on their star formation, together with the derived lopsidedness of the star formation distribution, the radial color gradients and other morphological parameters, show that these galaxies are characterized by modest total star formation rates (SFR), typically $\sim 7 \times 10^{-3}$ M$_\odot yr^{-1}$, concentrated at a few (1–5) small and faint star formation regions, which are randomly and asymmetrically distributed throughout the disk.

One appealing picture describing the star formation history of LSB-dIs is that we

are witnessing a quiescent phase in a star-bursting galaxy. By definition, a starburst is a localized and intense event, whereby the formation of stars in a galaxy is proceeding at a far greater rate than in the recent past (Weedman 1986). At the other extreme of particular interest in LSB-dIs is the case of a galaxy which shows faint signatures of current star formation. In this case, massive stars may not dominate the total energy emitted by the galaxy and the remnants of previous generation of stars may provide the dominant contribution to the optical continuum. This is because the integrated color of a star forming galaxy depends on the ratio of the mass of the stars formed during the recent star formation to the mass of the old stellar population. The question whether the current rate of star formation in Virgo LSB-dIs was typically low and steady during a Hubble time (constant star formation model) or if the current star formation rate indicates a post-burst galaxy (bursting model) is the main motivation of this paper.

In the following sections the observational and theoretical limitations inherent in modeling these type of galaxies are reviewed. Model analyses are carried out by comparing the Hα luminosity and the broad-band UBVRI colors, as galaxy integrated quantities, to predictions from published libraries of evolutionary synthesis models. The metallicity and the age of these galaxies can, therefore, be constrained. The relative contributions of the different stellar populations are investigated. Results are discussed and conclusions are presented at the end of the paper.

3. Observational and Theoretical Limitations

The past several years have witnesses the developments of various techniques to derive the star formation history of galaxies. The general concept is based on the fact that, at the early phase of a star formation event, hot stars emit copious amounts of ultraviolet (UV) and visible continuum photons. Although a similar phase of high effective temperature occurs near the completion of the life of a star (*e.g.* , blue

horizontal branch stars) the contribution to the UV continuum of the young stars is larger by orders of magnitude. Emission lines are produced when these UV photons ionize and excite nearby gas. The dust connected with the star formation region is heated by the strong stellar radiation and re-radiates a strong infrared continuum. Non-thermal continua are produced by supernova remnants. Observationally, such a young galaxy may be recognized as having blue colors, strong nebular emission-line spectrum, high inferred supernova rate, and (if dust is present) a high infrared luminosity (Leitherer & Heckman 1995.) In principle, all these radiation mechanisms can be related to the number and properties of the massive stars involved in the starburst and, by extrapolation to low-mass stars, a star formation history can therefore be derived.

Ideally, star formation histories should be derived directly from spectroscopy of resolved stars. Our sample of LSB-dIs is comprised of objects that are too faint and too distant to allow the use of such technique. The only possible approach at this time is to use integrated and/or surface photometry, but then, the number of available observational parameters is limited. The use of optical colors as a tracer of the star formation history relies on color indices that are largely degenerate with age and metallicity (Worthey 1994). For example, blue colors may imply low metallicity (Z). However, Z may be intrinsically low because metals could have been lost in a past burst of star formation by supernova-driven winds, or the gas could have been lost by the galaxy in a starburst event and part of it could have been subsequently accreted to replenish the galaxy gas supply. It is also possible that blue colors are the result of a truncated initial mass function (IMF) in the past, whereby only high mass ($> 10M_{\odot}$) stars were formed in a burst. According to Worthey, the ratio of the percentage change in age to the percentage change in metallicity is roughly the same for all optical colors (for example $\frac{\Delta age/age}{\Delta Z/Z}$ is 1.5 for U-V, 1.4 for B-V and V-I, and 1.3 for V-R). Larger numbers indicate greater metallicity sensitivity. Obviously, broad-band colors alone cannot discriminate between effects of age and metal abundance.

Balmer lines are less metallicity-sensitive than optical colors ($\frac{\Delta age/age}{\Delta Z/Z} \sim 0.6$). Kennicutt (1983) pointed out that a combination of broad-band data with Hα can provide useful information about star formation histories. In these cases, dust extinction in the Hα line should be taken into account to estimate accurately ages of stellar populations. Other problems arise in that both dust and aging of the stellar populations redden a galaxy's spectral energy distribution (SED) in the same direction. For instance, Gordon, Calzetti & Witt (1997) suggested that the reason for the absence of starbursts with ages < 8 Myr may be that, in the initial phases, the starburst is hidden by dust clouds and it is difficult to observe.

Other limitations arise because state-of-the-art evolutionary synthesis models, to which color indices have to be fitted, are most sensitive to massive stars. Mas-Hesse & Kunth (1991) noted that only in the context of a single stellar population (**SSP**) a global analysis allows the reduction of the age error to ~ 10 Myr. The reason is that the time needed for the proto-stellar collapse of a low-mass interstellar matter (ISM) cloud is at least several million years, which is, in any case, longer than the time required for the formation of the most massive stars. The **SSP** approximation works well for dating starbursts in galaxies where the light is mostly dominated by the current burst, as in high surface brightness (HSB) galaxies. But in LSB-dIs, where the star formation rate is very low, the very different age of the stellar populations can make this approximation uncertain. Finally, although the latest generation of evolutionary models has been largely improved (an overview of the latest achievements can be found in the conference volume edited by Leitherer *et al.* 1996), the dust influence on the parameters is uncertain and neither the metallicity nor the IMF are allowed to vary as function of time in these models. As to what extent these effects may be sources of errors and could affect the spectral energy distribution will remain unknown, until the publication of new generations of theoretical models.

4. Stellar Evolutionary Synthesis Models

State-of-the-art evolutionary synthesis models for galaxies are characterized by two principal parameters: the initial mass function (IMF) and the star formation rate (SFR). The IMF defines the number of stars formed per unit stellar mass and describes the mass-weighted proportion of massive stars to low-mass stars formed in a burst. The IMF is defined between a lower mass limit M_{low} and an upper mass limit M_{up}. The IMF is generally expressed as a power law

$$dN = N_\circ m^{-\alpha} dm$$

The normalization constant $N_\circ$ is determined by the total gas mass converted into stars, and the exponent α controls the shape of the IMF. Salpeter (1955) estimated $\alpha = -2.35$ for the solar neighborhood, but other IMF types were are also considered; for example Miller & Scalo (1979) derived a steeper slope $\alpha = -3.3$ and proposed a piecewise IMF with different α for specific mass ranges.

The SFR characterizes the intensity of the starburst and corresponds to the number of massive stars formed per unit time during one episode of star formation This function is expressed as :

$$\phi(t) = \phi_\circ e^{-t/\tau}$$

where $\phi_\circ \equiv \phi(t = 0)$, t is the age and τ is the e-folding time of the burst. In principle, by assuming a specific function for the IMF, the integrated SFR can be extrapolated to lower masses. If a burst is short compared to the age of a galaxy, all stars can essentially be considered coeval; this is the case of a single stellar population (**SSP**), some times called "instantaneous burst" of star formation (**IB**). Another case is that in which the star formation proceeds continuously at a constant rate (**CON**). Models with longer decay times τ of this family of models have bluer colors for the same age of the stellar population. While the second case (**CON**) is characteristic for

large systems with numerous individual HII regions as well as for most isolated dwarf irregular galaxies (van Zee, 2001), simple mathematical rules do not always fit the time dependence of the star formation in dIs and composite stellar populations (**CSP**) must be considered (Almoznino & Brosch 1998, thereafter AB98).

Evolutionary synthesis models provide different IMFs and star formation histories over a wavelength range extending from the ionizing UV to the near-infrared. The color evolution in a **SSP** model may be simplistically summarized as follows: At the first stage of star formation, and during the first 3 Myr, there is little color evolution because the colors of hot stars are insensitive to temperature changes. The colors are similar to those of individual O and early-B stars. An additional nebular contribution at early stages makes all colors redder, with the exception of U–B; this is because the U filter includes the Balmer edge where nebular hydrogen produces strong recombination lines. If M_{up} is reduced, at $t < 5$ Myr all colors but U–B become bluer because the nebular continuum is weaker. The same effect occurs when a steeper slope α is adopted. The explanation of this apparent paradox is that, in this case, massive stars generate smaller numbers of ionizing photons. At 10 Myr all colors are strongly reddened due to the appearance of red supergiant stars (RSG). Changes in metallicity strongly influence the relative number of RSG stars in the sense that low metallicity yields bluer RSG stars (less metal-blanketing). O-stars with low metallicity live longer, because their cooling is slower. After $\sim$ 10 Myr, the most massive stars have evolved off the main sequence and became red supergiants, making the UV light drop and the near-infrared light rise. At about 20 Myr the O-stars disappear and all colors are near constant or gradually reddening. For the next few tens of Myrs. the equivalent widths of emission lines are not longer measurable. From about 100 Myr the red giant branch takes over the production of the near-infrared light. Finally, at the end of the burst, after about 1 Gyr, a galaxy will appear redder, richer in dust, with more molecular gas than at the beginning of the burst, and will have a higher metallicity. Models with constant SFR or with longer decay

times have bluer colors for the same age of the stellar population as already mentioned, because of the dominance of young massive stars.

In this paper we refer specifically to the models of Worthey (W94, 1994), Leitherer *et al.* (LH99=STARBUST 99, 1999), Cervino, Mas-Hesse & Kunth (CMHK, 2001), and Bruzual & Charlot (1993, 1995, BC95 ≡ GISSEL). GISSEL is referred to as the Galaxy Isochrone Synthesis Spectral Evolution Library. W94 concentrates on intermediate and old stellar populations, between 1.5 and 17 Gyr of age. The range of metallicities considered is 0.0001 to 0.1, the lower mass cutoff is $M_{low} = 0.1M_{\odot}$ and the upper mass cutoff is $M_{up} = 2M_{\odot}$. LH99 optimizes stellar evolutionary synthesis of massive stars and includes the associated nebular emission but lacks information about stages of stellar evolution later than 1 Gyr. The mass range is 1–100$M_{\odot}$, the assumed metallicity values are Z=0.040, 0.020 ($Z_{\odot}$), 0.008, 0.004, and 0.0001. The model computes also a truncated IMF with $M_{up} = 30M_{\odot}$. The CMHK grids focus on the evolution of massive stars during the first 20 Myr. The model comprises five values of metal abundance in the range Z=2$Z_{\odot}$ to Z=$Z_{\odot}$/20, a validity range between 2 and 120$M_{\odot}$, and slopes α=1, 2.35, and 3. BC95 is an improved version of the stellar population synthesis models originally described in Bruzual & Charlot (1993). The library adopts a mass range of 0.1-125$M_{\odot}$, extends to 20 Gyr, but lacks information on the nebular continuum. We refer the reader to the original papers for more details in the description of the models.

5. Color-Color Diagrams

In this section we test our results against the model predictions by plotting in color-color diagrams the measurements, together with tracks representing different ages as predicted by single metallicity theoretical models.

The plot in Fig. 1 shows the color-color diagram of (U–B) *vs.* (B–V) and the experimental points are labeled with the galaxy names, and are plotted together with some **LH99** and **BC95** models. The **LH99** models for Z=0.02, 0.008, and 0.001 metallicity are represented by solid-thin lines. The **BC95** calculations, for $Z_{\odot}$ (Z=0.02), are plotted with thick lines and consist of four types of components: (1) exponentially decaying SFR with 1 Gyr decay times (τ 1Gyr, short-dashed line); (2) instantaneous burst of star formation (SSP, long-dashed line); (3)burst of star formation lasting 1 Gyr (CSP 1Gyr, dot-dashed line); (4) continuous star formation (CON, dotted line). Fig. 2 shows diagrams of (U–B) *vs.* (V–I) with **LH99** and **BC95** models as in Fig. 1. Fig. 3 shows the diagrams for (U–V) *vs.* (V–I). Fig. 4 shows the diagrams for (U–B) *vs.* (V–R). Fig. 5 shows the diagrams for (B-V) *vs.* (V–I) and includes the AB98 sample of BCDs that are Virgo cluster members. Figures 6 and 7 show color-color diagrams of (Hα–V) *vs.* (B–V) and (Hα–V) *vs.* (U–B) respectively, with the **CMHK** (Z=0.001, 0.008, 0.02) and **BC95** (Z=0.02) models.

Due to advantages such as the use of integrated colors, a global analysis is generally performed to derive a typical mode of star formation in a galaxy. However, this approach lacks flexibility in assigning different metallicity and/or aging differences across the structure. We emphasize the large asymmetries and radial color fluctuations found in our sample Heller *et al.* (2000, 2001) that may lead to a misleading evolutionary interpretation. While we minimize this effect by taking as typical colors the median colors derived from surface brightness radial profiles instead of global average colors, such a bias is inherent in the large dispersion of the data set plotted in the diagrams. For example, in (U–B) the standard deviation σ_{U-B} can reach up to 0.60 magnitudes, due to the high sensitivity of this band-pass to the young population. The other standard deviations are $\sigma_{B-V} \leq 0.42$, $\sigma_{V-I} \leq 0.40$ $\sigma_{V-R} \leq 0.33$.

To derive a typical mode of star formation for each galaxy we define a fit-deviation

parameter Δ as the perpendicular distance from the location of the observed data point in the diagrams to the line of evolution of a specific theoretical model. In Table 1 we list, for each galaxy, the measured Δ parameters (in magnitude units) in representatives diagrams with respect to the models enclosing the entire sample. The smallest Δ for each galaxy is an indication of the best-fitted model of the list. For the **SSP** models we measured Δ for three metallicities: Z=0.001, 0.008, and 0.02, listed from left to right. For **CON,** τ **1 Gyr**, and **CSP 1Gyr** models we measured Δ for $Z_{\odot}$.

One may expect that galaxies with short e-folding star formation τ parameters, or galaxies which are dominated by a single bust of star formation (**SSP** model), where the SF burst happened more than one Gyr ago, will have evolved into extremely red galaxies by the present epoch. In contrast, galaxies with long τ parameters or constant star formation (**CON**) will appear as blue systems even after a Hubble time. Most remarkable for such a homogeneous sample of galaxies (considering the selection criteria) is the large scatter of the observed colors in the plots. A common characteristic, at young and median ages in all the plots, is that the entire set tends to be displaced upward and to the right from the predicted line of evolution of **SSP** models. However, the points are too dispersed to derive a general conclusion for the entire sample as having blue colors, as defined by the constant star formation model. This leads to the conclusion that **SSP** models should not be considered independently in the evolutionary study of such structures as LSB-dIs but that the possible explanation may be a combination of **SSP**s.

Regarding the IMF parameters, we found that increasing the slope α, or lowering M_{up}, worsens the fit. Lowering M_{up} from 100 to 30 $M_{\odot}$ at the early SF phase has less dramatic consequences than steepening the IMF from -2.35 to -3.3. This means that a truncated IMF cannot explain the SF process in LSB-dIs. LH99 assert that for relative quantities, such as color indices, M_{low} has no effect when considering wavelengths and ages that are dominated by higher mass stars; this seems to be the case for our sample.

Color-color diagrams that combine broad-band colors and/or Hα, where one band is common in both the x and the y-axis, provide useful tools to interpret the relative flux contribution of composite populations. For example, in a simple scenario of two populations, their relative contribution to the composite population can be calculated by a weighting scheme (AB98). The result of the combination lies on a line connecting two points in the color-color diagrams. Having a common band in the two color indices is necessary, since the ratio of the fluxes of the two populations is measured relative to their light contribution in this common band. Basically, by defining the ratio between two populations "1" and "2" fluxes by a factor k:

$$k = \frac{I_{2V}}{I_{1V}}$$

the combined color index between a certain spectral band λ and the common band V (for example) is given by:

$$(\lambda - V) = -2.5 \log \left(\frac{10^{-0.4(\lambda - V)_1} + k\, 10^{-0.4(\lambda - V)_2}}{1 + k} \right)$$

We calculated combined color indices for two populations relative to the V-band and using k values of 0.1, 0.25, 1, 5, and 10. We added examples of such combinations for 10 Myr+10 Gyr and 15 Myr+5 Gyr in Figure 6 [the diagram (Hα –V) *vs.* (B–V)]. Another example of combined populations of 10 Myr+5 Gyr, for (U-V) *vs.* (V-I) is displayed in Fig. 3. It is evident from these plots that the relative flux of the two populations depends strongly on the metallicity assigned to a galaxy. In general, $k > 1$ when fitting to models with $Z_\odot$, but $k \sim 1$ (roughly equal contributions of the two populations) using models with $Z < Z_\odot$. A summary of the relative contributions of the current to the recently formed stars, for the best-fitted metallicities, is listed in Table 2.

6. Conclusions

We have investigated here the relation between the Hα luminosity and the broad-band colors in the context of evolutionary models. The results show that Virgo cluster member galaxies that are LSB-dIs do not have the red colors expected from post-starburst galaxies, neither do they show the dominant blue color expected for constant star formation models. They appear to have had a multiple and episodic star formation history that resulted in composite stellar populations during a Hubble time, similar to what Almoznino & Brosch (1998b) found for BCD galaxies. Despite the fact that a few of the galaxies in the sample may be classified as post-bursting objects, the lack of Hα spatial concentration and the color gradients characteristic of bursting galaxies makes this interpretation less confident.

Given their low SFRs, it is not surprising that LSB-dIs are no fitted by SSP bursting models. It is interesting to note that starbursts were reported to be exceptional cases in the dI category (van Zee 2001), in accordance with our results. The IMF parameters, can be fitted by different metallicities ranging from 0.001 to 0.02, a Salpeter $\alpha = -2.35$ and $M_{up} \sim 100 M_{\odot}$.

REFERENCES

Almoznino E., Brosch N., 1998, MNRAS, 298, 920 (AB98)

Almoznino E., Brosch N., 1998b, MNRAS, 298, 931

Bruzual A. G. & Charlot S., 1993, ApJ, 405, 538

Bruzual A. G. & Charlot S., 1995, available at web site http://www.stsci.edu.instruments/observatory/cdbs/

Cervino M., Mas-Hesse J. M & Kunth D., 2001, A&A, (submitted) (http://www.laeff.esa.es/ mcs/model)

Gordon K. D., Calzetti D., & D. Witt A. N.,1998, AJ, 115, 1438

Heller A. B., Almoznino E., Brosch N., 1998, in Davies J. I, Impey C., Phillipps S., ed., ASP Conf. Ser. Vol. 170, The Low Surface Brightness Universe, Astron. Soc. Pac., San Francisco, p. 282

Heller A. B., Almoznino E., Brosch N., 1999, MNRAS, 304, 8

Heller A. B., Brosch N., Almoznino E., Van Zee L., Salzer J. J., 2000, MNRAS, 316, 569

Heller A. B. & Brosch N., 2001, MNRAS, in press.

Kennicutt R. C., 1983, ApJ, 272, 54

Leitherer C. Fritze-v. Alvensleben U., & Hunchra J., 1996, From Stars to Galaxies - The Impact of Stellar Physics on Galaxy Evolution (San Francisco: ASP)

Leitherer C. & Heckman T., 1995, ApJS, 96, 9

Leitherer C., Schaerer D., Goldader J. D, Gonzales Delgado R. M., Robert C., Kune D. F., Mello D. F. , Devost D., and Heckman T. M., 1999, ApJSS, 123, 3

MacLow M. M. & Ferrera A., 1999, ApJ, 513, 15

Mas-Hesse J. M & Kunth D., 1991, Astron. Astrophys. Suppl. 88, 399

Miller G. E. & Scalo J. M., 1979 ApJS, 41, 513

Salpeter E. E., 1955 ApJ, 121, 161

van Zee L., 2001, ApJ, 121, 2003

Weedman D.W., Quasar astronomy, 1986, Pringe J. E, Davies R. L. & Efstathiou E., ed., Cambridge University Press

Worthey G., 1994, ApJS, 95, 107

This manuscript was prepared with the AAS LaTeX macros v4.0.

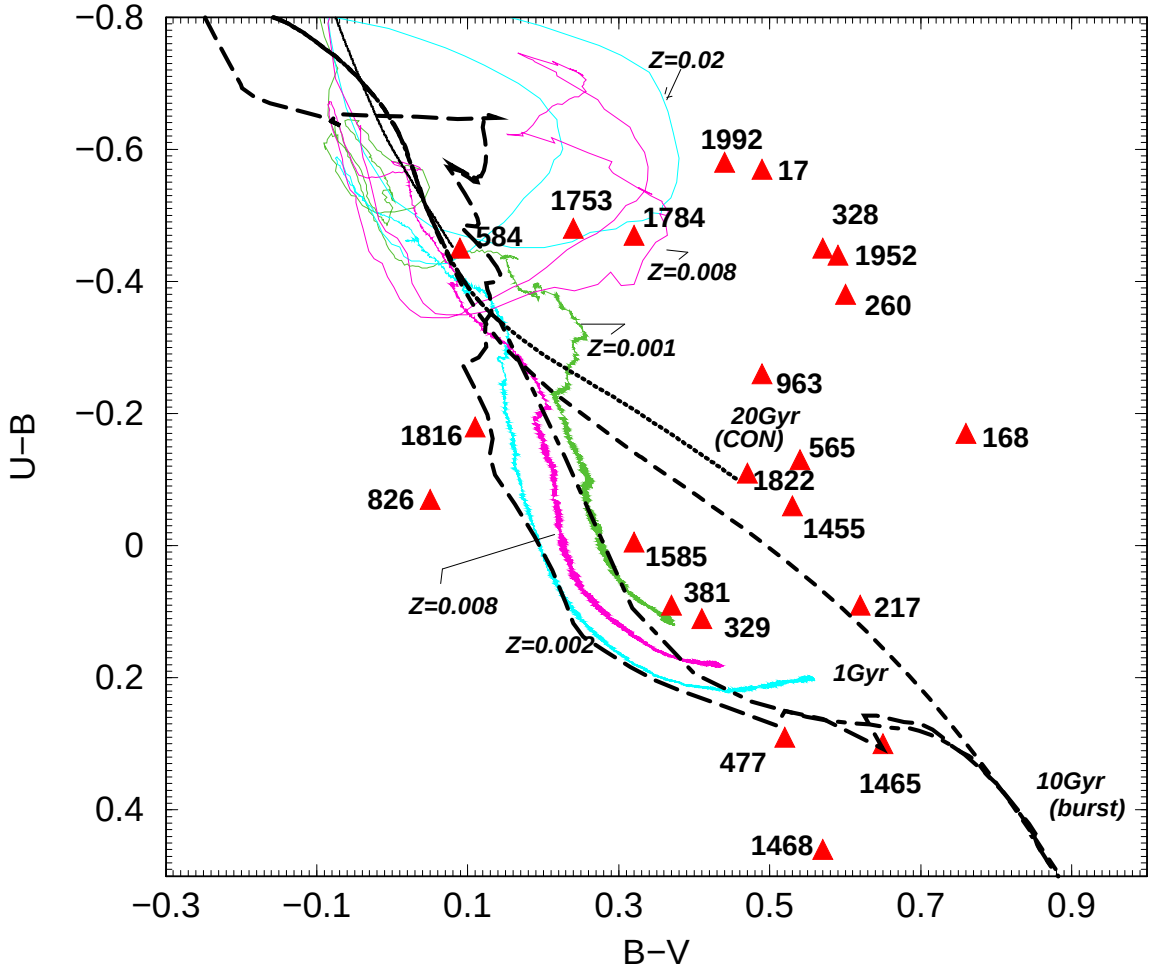

Fig. 1.— Color-color diagrams of (U-B) *vs.* (B-V). The individual galaxies are labeled with their VCC name. The LH99 models for Z=0.001, 0.008, and 0.02 metallicities are represented by solid-thin lines. The BC95, for metallicity Z=0.02, are represented by thick lines and consist of four types of components: 1) exponential decaying SFR with 1 Gyr decay times (τ 1Gyr, short-dashed line); 2) instantaneous burst of star formation (SSP, long-dashed line); 3)burst lasting 1 Gyr (CSP 1 Gyr, dot-dashed line); 4) continuous star formation (CON, dotted line)

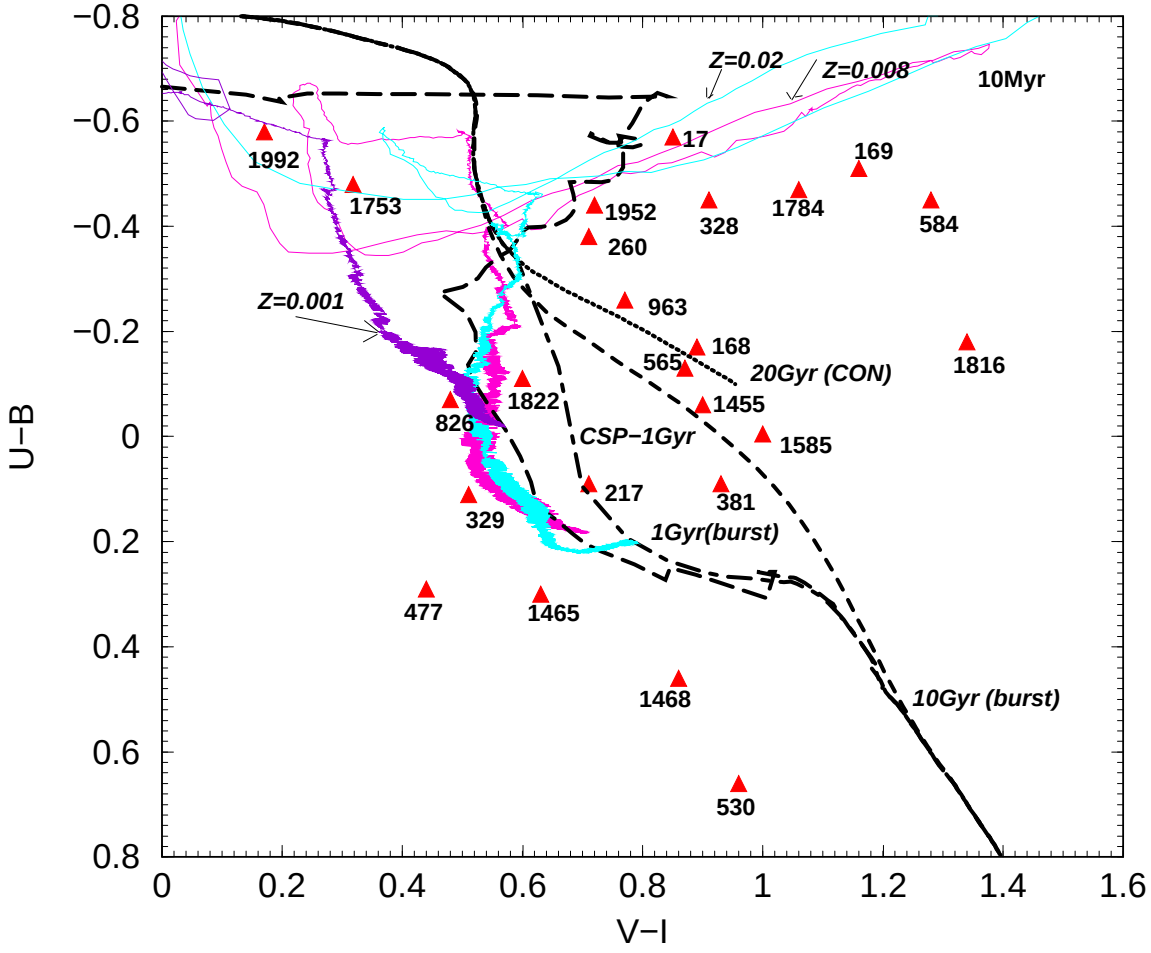

Fig. 2.— Color-color diagrams (U-B) *vs.* (V-I). LH99 models for Z=0.001, Z=0.008 and Z=0.02. BC95 models as Fig.1

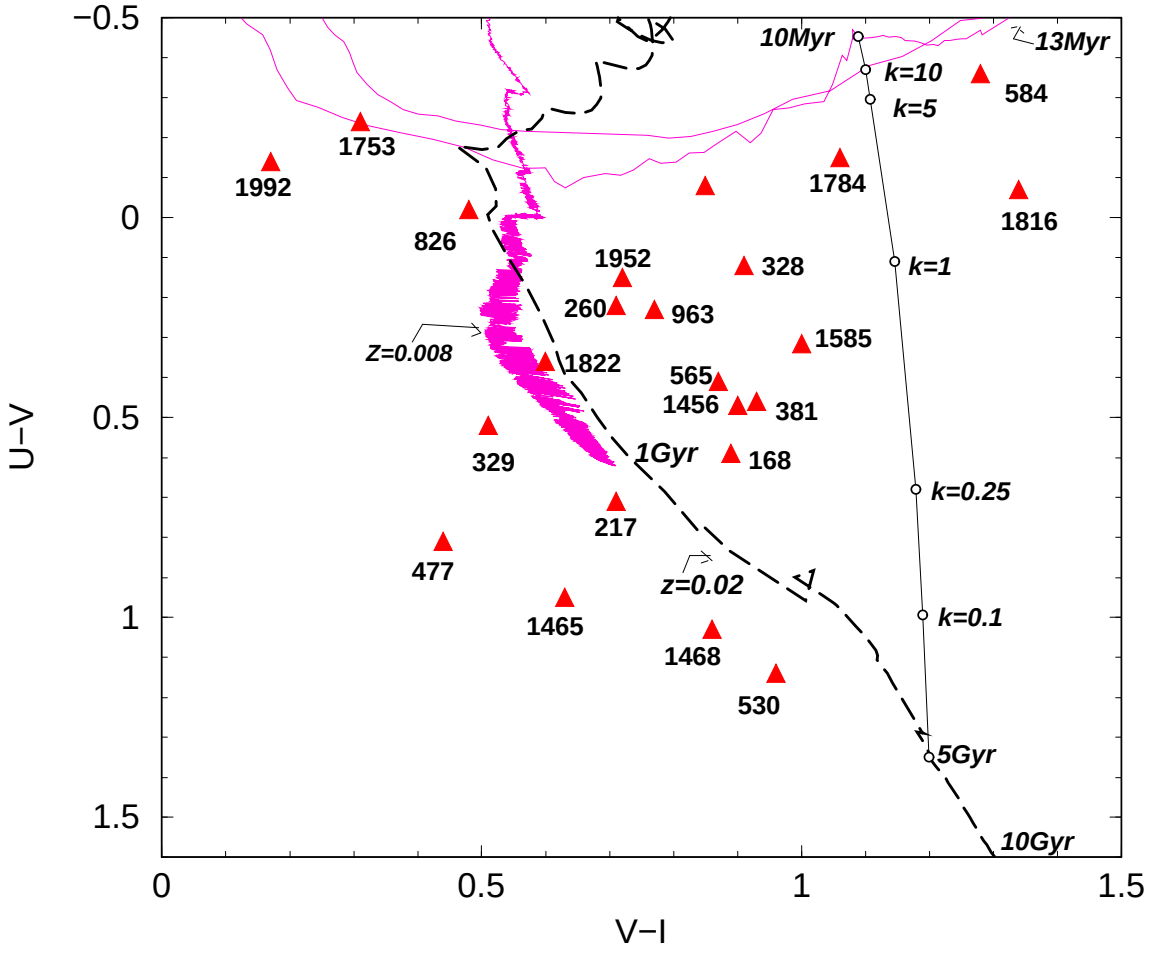

Fig. 3.— Color-color diagrams (U-V) *vs.* (V-I). Models LH99 (Z=0.008), BC95 (Z=0.02) and combined weighted schemes (AB98). For the latter, k=1 implies an equal contribution in the V band from a 10 Myr population and a 5 Gyr population.

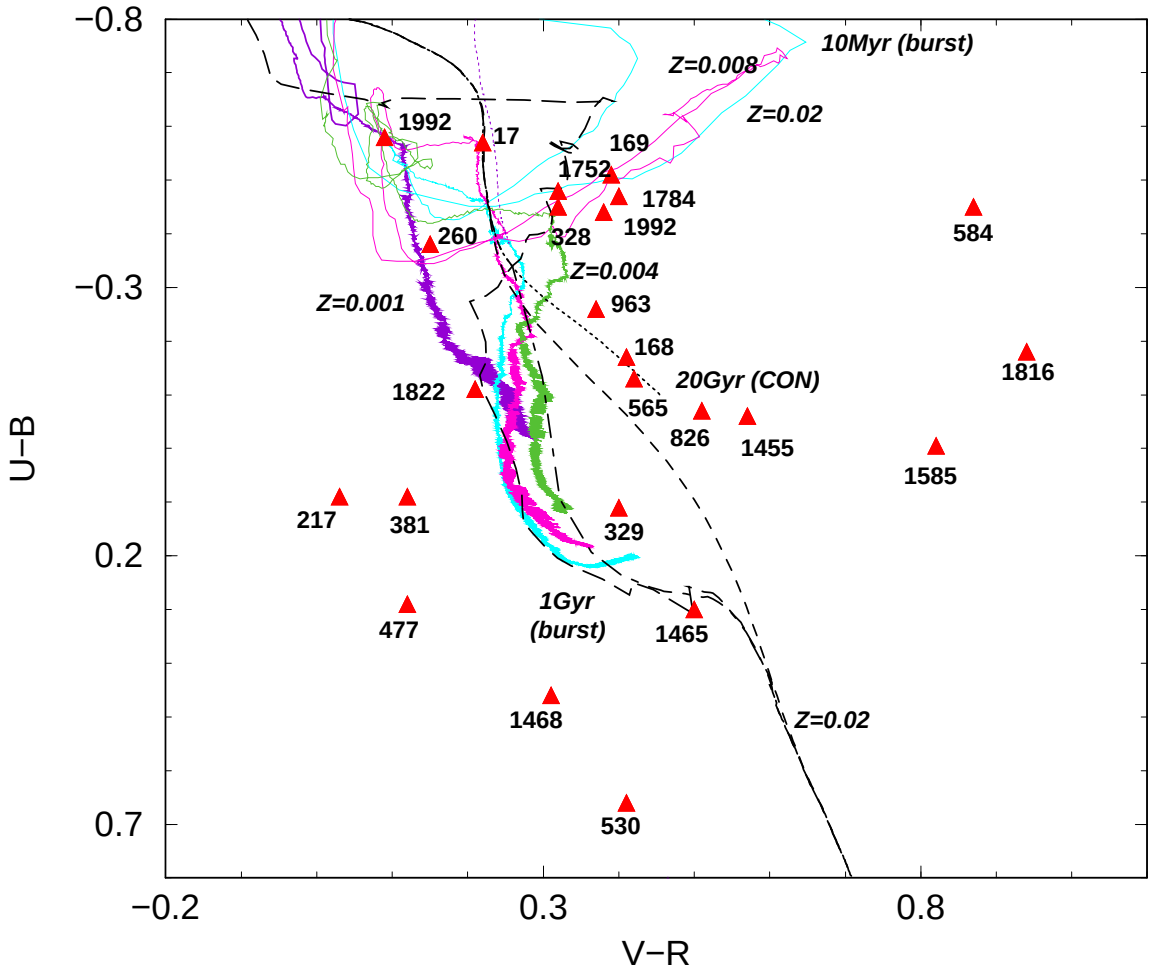

Fig. 4.— Color-color diagrams (U-B) *vs.* (V-R). Models LH99 (Z=0.001,Z=0.004, Z=0.008 and Z=0.02). BC95 models as Fig.1

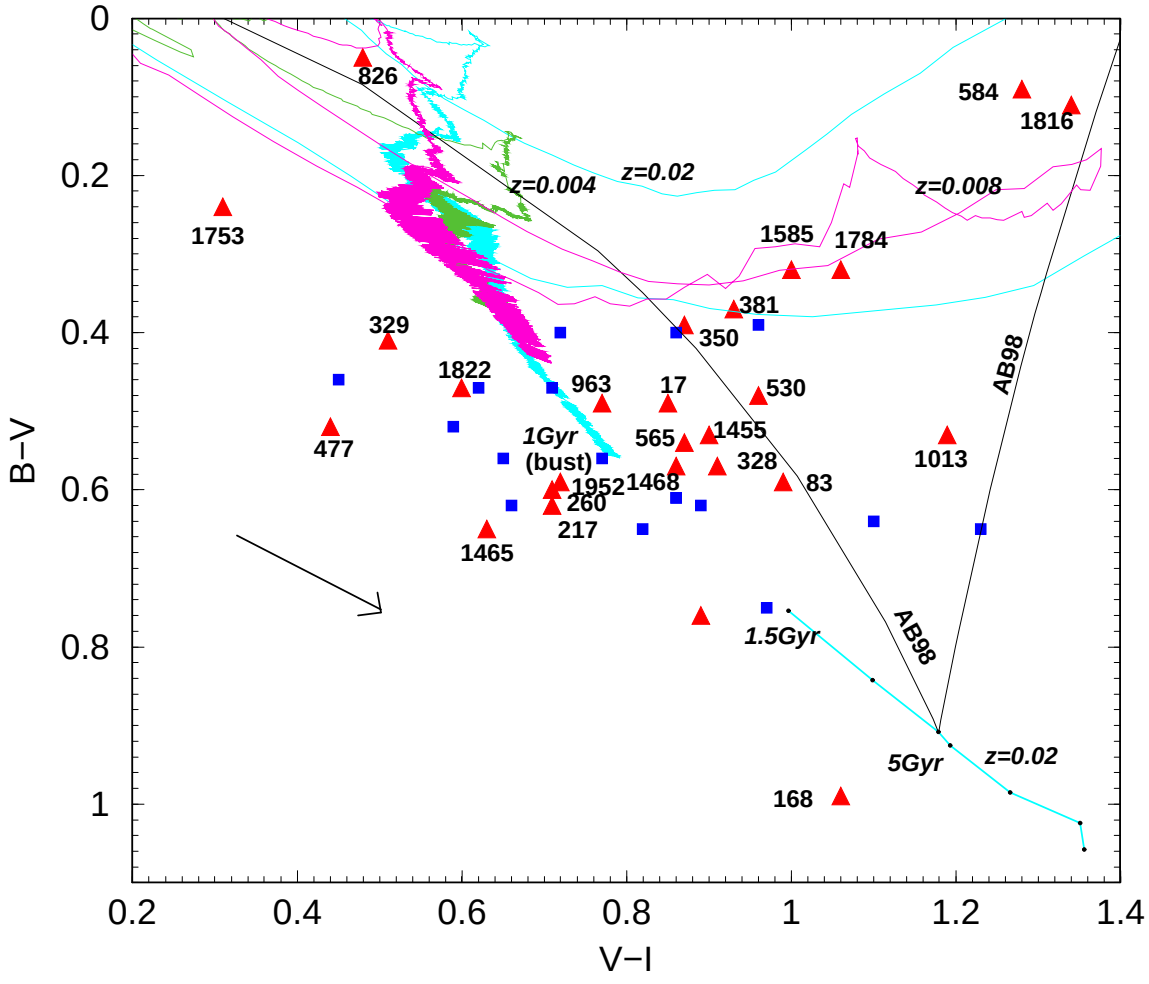

Fig. 5.— Color-color diagrams (B-V) *vs.* (V-I). Models LH99 (Z=0.004, 0.02) and W94 (Z=0.02). Squares symbols represent BCDs from AB98. The arrow indicate the direction of dust extinction for $A_V/E(B_V) = 3.1$.

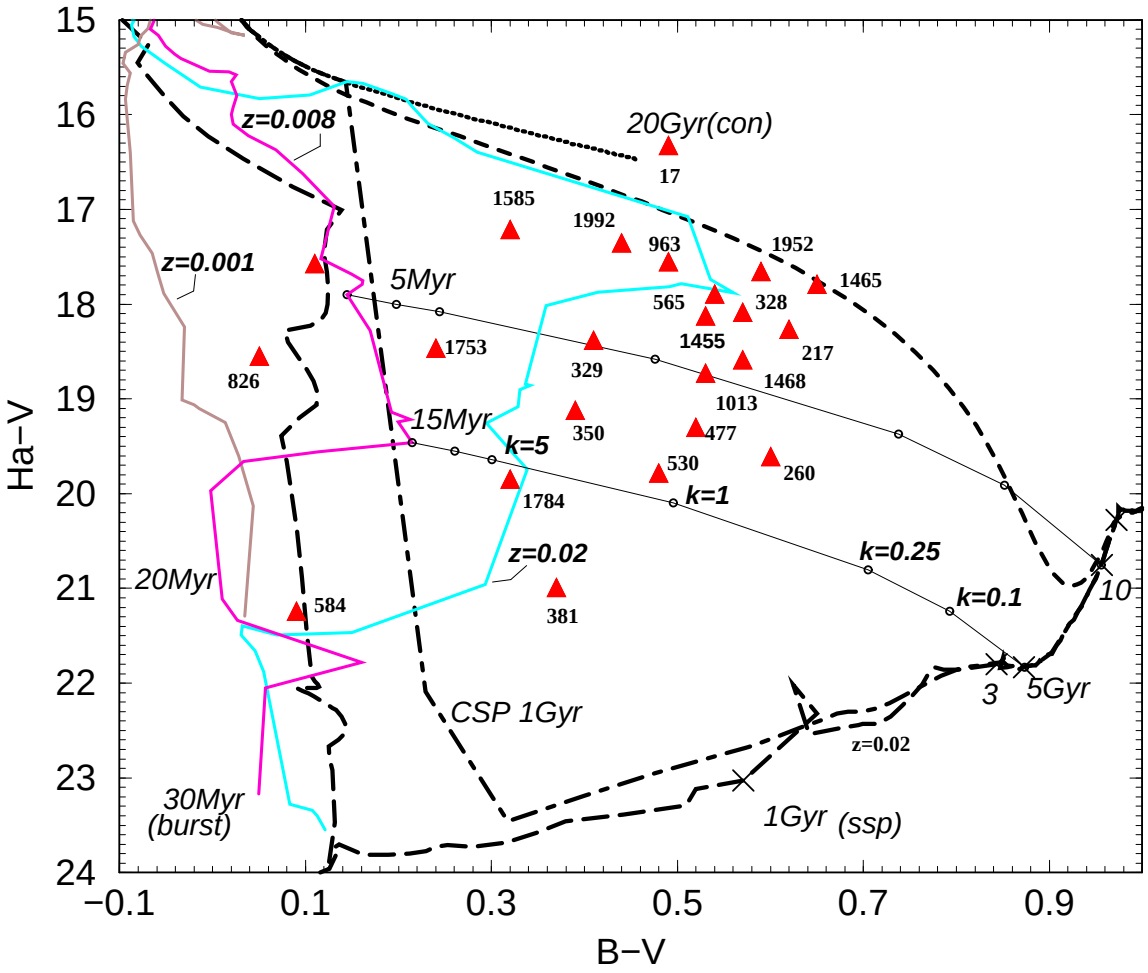

Fig. 6.— Color-color diagrams (Hα-V) *vs.* (B-V). Models CMHK (Z=0.001, 0,008, 0.02), BC95 (Z=0.02) and combined weighted schemes (AB98).

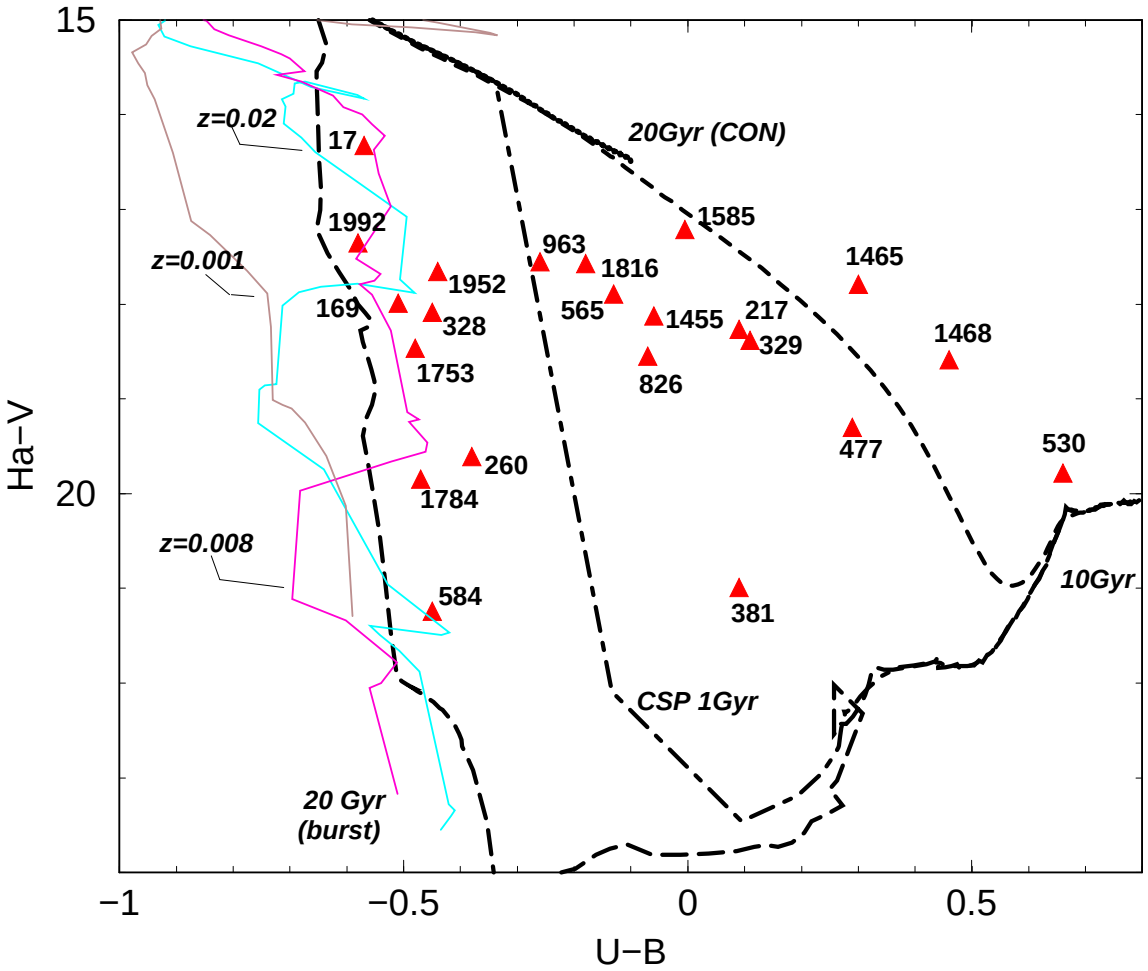

Fig. 7.— Color-color diagrams (Hα-V) *vs.* (U-B). Models CMHK (Z=0.001, 0,008, 0.02) and BC95 (Z=0.02).

Table 1. Fit deviation Δ

VCC	mode	U-B *vs.* B-V	U-B *vs.* V-I	B-V *vs.* V-I	(Ha-V) *vs.* (B-V)	(Ha-V) *vs.* (U-B)
17	CON	0.25	0.34	0.13	0.10	1.2
17	SSP	0.24 0.14 0.10	0.56 0.01 0.01	0.10 0.10 0.10	0.59 0.40 0.20	0.35 0.02 0.06
17	τ 1Gyr	0.28	0.33	0.10	0.70	1.2
17	CSP 1Gyr	0.24	0.34	0.01	0.33	0.25
...	...	...	...	...	...	...
168	CON	0.32	0.05	0.36		
168	SSP	0.58 0.55 0.60	0.36 0.36 0.36	0.20 0.20 0.20		
168	τ 1Gyr	0.40	0.12	0.23		
168	CSP 1Gyr	0.52	0.24	0.20		
...	...	...	...	...	...	...
169	CON		0.54			2.8
169	SSP		0.80 0.12 0.12			0.22 0.020 0.04
169	τ 1Gyr		0.58			0.6
169	CSP 1Gyr		0.58			0.24
...	...	...	...	...	...	...
217	CON	0.26	0.32	0.40	1.8	1.5
217	SSP	0.10 0.14 0.16	0.01 0.01 0.01	0.15 0.15 0.13	0.66 0.44 0.26	0.63 0.63 0.63
217	τ 1Gyr	0.03	0.24	0.32	1.0	0.7
217	CSP 1Gyr	0.21	0.01	0.23	0.45	0.15
...	...	...	...	...	...	...
260	CON	0.32	0.10	0.37	3.5	3.1
260	SSP	0.37 0.27 0.27	0.40 0.14 0.14	0.15 0.15 0.13	0.57 0.51 0.27	0.24 0.29 0.08
260	τ 1Gyr	0.36	0.10	0.32	2.2	3.1
260	CSP 1Gyr	0.44	0.10	0.23	0.31	0.17
...	...	...	...	...	...	...
328	CON	0.34	0.26	0.17	1.6	2.7
328	SSP	0.33 0.22 0.24	0.60 0.10 0.12	0.04 0.04 0.04	0.60 0.42 0.22	0.28 0.08 0.26
328	τ 1Gyr	0.40	0.26	0.04	1.0	2.7
328	CSP 1Gyr	0.46	0.26	0.01	0.43	0.16
...	...	...	...	...	...	...
329	CON	0.22	0.45		2.6	1.6
329	SSP	0.01 0.04 0.08	0.01 0.01 0.01	0.15 0.15 0.15	0.42 0.25 0.06	0.72 0.72 0.62
329	τ 1Gyr	0.16	0.40	0.31	2.3	0.80
329	CSP 1Gyr	0.06	0.18	0.24	0.25	0.19
...	...	...	...	...	...	...
350	CON			0.01	3.5	
350	SSP			0.20 0.03 0.03	0.38 0.18 0.08	

Table 1—Continued

VCC	mode	U-B *vs.* B-V	U-B *vs.* V-I	B-V *vs.* V-I	(Ha-V) *vs.* (B-V)	(Ha-V) *vs.* (U-B)
350	τ 1Gyr			0.03	3.2	
350	CSP 1Gyr			0.10	0.18	
...	...	...	...	...	...	...
367	CON	1.5	1.5	0.55		
367	SSP	0.20 0.20 0.20	0.45 0.45 0.45	0.30 0.30 0.30		
367	τ 1Gyr	0.20	0.45	0.30		
367	CSP 1Gyr	0.20	0.45	0.30		
...	...	...	...	...	...	...
381	CON	0.23	0.18	0.05	4.7	4.5
381	SSP	0.01 0.03 0.07	0.20 0.20 0.20	0.03 0.03 0.03	0.32 0.36 0.08	0.54 0.54 0.50
381	τ 1Gyr	0.17	0.08	0.10	4.3	3.4
381	CSP 1Gyr	0.04	0.18	0.13	0.15	0.20
...	...	...	...	...	...	...
477	CON	0.41	0.62	0.55	3.0	3.0
477	SSP	0.08 0.05 0.03	0.24 0.24 0.24	0.32 0.32 0.32	0.49 0.30 0.20	1.0 1.0 0.76
477	τ 1Gyr	0.18	0.58	0.51	2.7	0.7
477	CSP 1Gyr	0.02	0.34	0.41	0.31	0.10
...	...	...	...	...	...	...
530	CON	0.90	0.78	0.03	3.4	3.5
530	SSP	0.35 0.35 0.35	0.29 0.29 0.29	0.22 0.22 0.22	0.42 0.43 0.15	1.28 1.28 1.11
530	τ 1Gyr	0.35	0.31	0.02	3.1	0.3
530	CSP 1Gyr	0.35	0.31	0.10	0.27	0.80
...	...	...	...	...	...	...
565	CON	0.07	0.08	0.15	1.7	1.6
565	SSP	0.30 0.33 0.48	0.34 0.34 0.34	0.11 0.11 0.11	0.68 0.45 0.10	0.61 0.43 0.56
565	τ 1Gyr	0.14	0.08	0.11	0.60	1.7
565	CSP 1Gyr	0.30	0.20	0.04	0.45	0.16
...	...	...	...	...	...	...
584	CON	0.01	0.50	0.54	5.8	6.0
584	SSP	0.01 0.01 0.01	0.86 0.16 0.16	0.54 0.11 0.11	0.05 0.02 0.08	0.14 0.14 0.01
584	τ 1Gyr	0.01	0.56	0.50	5.8	6.0
584	CSP 1Gyr	0.01	0.76	0.52	0.10	0.27
...	...	...	...	...	...	...
826	CON	0.30	0.28	0.04	3.4	2.1
826	SSP	0.23 0.18 0.15	0.01 0.04 0.04	0.04 0.04 0.04	0.08 0.12 0.28	0.74 0.52 0.74
826	τ 1Gyr	0.24	0.26	0.04	3.4	2.1
826	CSP 1Gyr	0.23	0.26	0.04	0.04	0.25

Table 1—Continued

VCC	mode	U-B *vs.* B-V	U-B *vs.* V-I	B-V *vs.* V-I	(Ha-V) *vs.* (B-V)	(Ha-V) *vs.* (U-B)
...	...	...	...	...	...	...
963	CON	0.14	0.02	0.60	1.3	1.6
963	SSP	0.28 0.31 0.32	0.32 0.18 0.18	0.04 0.04 0.04	0.56 0.36 0.04	0.53 0.32 0.24
963	τ 1Gyr	0.20	0.12	0.25	0.40	1.6
963	CSP 1Gyr	0.31	0.20	0.04	0.31	0.01
...	...	...	...	...	...	...
1013	CON	0.08	0.08	0.14	2.4	
1013	SSP	0.25 0.30 0.32	0.28 0.28 0.28	0.35 0.35 0.35	0.56 0.34 0.16	
1013	τ 1Gyr	0.07	0.01	0.17	2.1	
1013	CSP 1Gyr	0.25	0.23	0.21	0.34	
...	...	...	...	...	...	...
1455	CON	0.08	0.08	0.13	1.8	1.6
1455	SSP	0.25 0.30 0.32	0.28 0.28 0.28	0.11 0.11 0.11	0.57 0.36 0.17	0.72 0.53 0.72
1455	τ 1Gyr	0.07	0.01	0.08	1.3	1.6
1455	CSP 1Gyr	0.25	0.23	0.03	0.37	0.27
...	...	...	...	...	...	...
1465	CON	0.46	0.44	0.40	1.6	0.5
1465	SSP	0.10 0.10 0.01	0.18 0.18 0.18	0.24 0.24 0.24	0.64 0.44 0.06	1.0 0.86 0.86
1465	τ 1Gyr	0.10	0.38	0.39	0.04	0.5
1465	CSP 1Gyr	0.01	0.18	0.30	0.42	0.7
...	...	...	...	...	...	...
1468	CON	0.58	0.30	0.20	2.2	1.0
1468	SSP	0.25 0.23 0.20	0.30 0.30 0.30	0.06 0.06 0.06	0.55 0.40 0.29	1.16 0.95 1.16
1468	τ 1Gyr	0.20	0.30	0.12	0.18	1.2
1468	CSP 1Gyr	0.03	0.30	0.02	0.29	0.7
...	...	...	...	...	...	...
1585	CON	0.17	0.12	0.13	1.20	0.40
1585	SSP	0.04 0.08 1.1	0.12 0.12 0.12	0.34 0.01 0.07	0.40 0.18 0.16	0.84 0.55 0.49
1585	τ 1Gyr	0.10	0.12	0.20	0.80	0.20
1585	CSP 1Gyr	0.04	0.31	0.15	0.16	0.29
...	...	...	...	...	...	...
1753	CON	0.17	0.20	0.37	2.8	2.9
1753	SSP	0.11 0.01 0.01	0.01 0.01 0.01	0.19 0.25 0.23	0.26 0.06 1.0	0.25 0.03 0.25
1753	τ 1Gyr	0.17	0.26	0.37	2.6	2.9
1753	CSP 1Gyr	0.17	0.26	0.37	0.06	0.22
...	...	...	...	...	...	...
1784	CON	0.21	0.40	0.20	3.80	4.6

Table 1—Continued

VCC	mode	U-B *vs.* B-V	U-B *vs.* V-I	B-V *vs.* V-I	(Ha-V) *vs.* (B-V)	(Ha-V) *vs.* (U-B)
1784	SSP	0.19 0.02 0.3	0.78 0.18 0.18	0.40 0.01 0.06	0.15 0.05 0.02	0.14 0.10 0.14
1784	τ 1Gyr	0.22	0.46	0.20	3.5	4.6
1784	CSP 1Gyr	0.22	0.46	0.14	0.13	0.26
...	...	...	...	...	...	...
1816	CON	0.17	0.48		2.0	1.6
1816	SSP	0.13 0.10 0.06	0.54 0.54 0.54		0.16 0.01 0.40	0.60 0.30 0.22
1816	τ 1Gyr	0.12	0.42		0.50	1.6
1816	CSP 1Gyr	0.10	0.64		0.10	0.10
...	...	...	...	...	...	...
1822	CON	0.10	0.18	0.30		
1822	SSP	0.23 0.26 0.28	0.10 0.10 0.04	0.10 0.10 0.10		
1822	τ 1Gyr	0.14	0.12	0.29		
1822	CSP 1Gyr	0.25	0.15	0.24		
...	...	...	...	...	...	...
1952	CON	0.36	0.15	0.10	0.5	2.2
1952	SSP	0.35 0.24 0.24	0.30 0.02 0.03	0.40 0.14 0.14	0.60 0.45 0.04	0.32 0.12 0.07
1952	τ 1Gyr	0.40	0.18	0.30	0.1	2.2
1952	CSP 1Gyr	0.46	0.02	0.20	0.45	0.17
...	...	...	...	...	...	...
1992	CON	0.38	0.22		1.0	2.0
1992	SSP	0.40 0.10 0.08	0.01 0.01 0.01		0.45 0.30 0.08	0.20 0.01 0.06
1992	τ 1Gyr	0.40	0.26		0.5	2.0
1992	CSP 1Gyr	0.40	0.08		0.34	0.29

Note. — Δ is given in magnitude units. For the **SSP** models Δ is given for three metallicities: Z=0.001, 0.008, and 0.02, and are listed from left to right. For **CON**, τ **1 Gyr**, and **CSP 1Gyr** models Δ is given for $Z_{\odot}$

Table 2. Model Predictions

VCC	Evolutionary synthesis model	Metallicity	Flux ratio 2 pop. model
17	SSP	0.02	$1-5$
83	SSP	0.02	< 0.01
168	SSP	0.02	< 0.01
169	SSP	0.008	> 10
217	SSP	0.02	$5-10$
260	SSP	0.02	$0.25-1$
328	SSP	0.008	$0.25-1$
329	CSP 1Gyr	0.02	$10-5$
350	SSP	0.02	$10-5$
367	τ 1Gyr or SSP	0.02	< 0.01
381	CSP 1Gyr	0.02	$10-5$
477	CSP 1Gyr	0.02	$1-5$
530	SSP	0.02	$0.25-1$
565	CSP 1Gyr	0.02	> 10
584	SSP	0.008	> 10
826	SSP	0.008	> 10
963	CSP 1Gyr	0.02	> 10
1013	SSP	0.02	$1-5$
1455	CSP 1Gyr	0.02	$1-5$
1465	SSP	0.02	$1-5$
1468	CSP 1Gyr	0.02	$1-5$
1585	CSP 1Gyr	0.008	$1-5$
1753	SSP	0.008	$5-10$
1784	SSP	0.008	> 10
1816	SSP	0.008	> 10
1822	SSP	0.008	< 0.1
1952	SSP	0.02	> 10
1992	SSP	0.02	> 10

Note. — K is the flux ratio of (Hα)–V *vs.* (B–V). Z is constrained by table 1